Spectroscopic Challenges of Photoionized Plasmas
ASP Conference Series, Vol. 247, 2001
Gary Ferland and Daniel Wolf Savin, eds.

Grains in Photo-Ionized Environments

P.A.M. van Hoof[1,2], J.C. Weingartner[1], P.G. Martin[1], K. Volk[3], and G.J. Ferland[2]

[1] *CITA, 60 St. George Street, Toronto, ON M5S 3H8, Canada*
[2] *University of Kentucky, 177 CP Building, Lexington, KY 40506, USA*
[3] *University of Calgary, 2500 University Dr. NW, Calgary, AB T2N 1N4, Canada*

Abstract. Ever since the pioneering study of Spitzer (1948), it has been widely recognized that grains play an important role in the heating and cooling of photo-ionized environments. This includes the diffuse ISM, as well as H II regions, planetary nebulae, and photo-dissociation regions. A detailed code is necessary to model grains in a photo-ionized medium since the interactions of grains with their environment include a host of microphysical processes, and their importance can only be judged by performing a complete simulation. In this paper we will use the spectral synthesis code Cloudy for this purpose. A comprehensive upgrade of the grain model has been recently incorporated in Cloudy, and certain aspects of this upgrade will be discussed. Special emphasis will be on the new grain charge model. We will consider in detail the physics of grains in both ionized and neutral environments, and will present a calculation of photo-electric heating and collisional cooling rates for a range of physical conditions and grain materials and for a range of grain sizes (including a realistic size distribution). We conclude with a brief discussion of the problems currently hampering progress in this field. The new grain model will be used to model the silicate emission in the Ney-Allen nebula, and will help us better understand the nature of the grains in that part of the Orion complex.

1. Introduction

Grains are ubiquitous in the interstellar medium (ISM), and they can be detected either directly through their far-infrared emission or indirectly through extinction or polarization studies. Despite the vast number of observations, many questions regarding grain composition and grain physics remain unanswered. Further study is therefore required, and detailed models are needed to interpret the results. Ever since the pioneering study of Spitzer (1948), it has been widely recognized that grains play an important role in the heating and cooling of the diffuse ISM (see also the more recent studies by Bakes & Tielens 1994, and Weingartner & Draine 2001a, hereafter WD). Grains also play an important role in the physics of H II regions and planetary nebulae (e.g., Maciel & Pottasch 1982, Baldwin et al. 1991, hereafter BFM, Borkowski & Harrington

1991, and Volk, these proceedings) and photo-dissociation regions (PDR's, e.g., Tielens & Hollenbach 1985).

The interactions of grains with their environment include a host of microphysical processes, and their importance and effects can only be judged by including all of these processes. This can, in turn, only be done with a complete simulation of the environment. In this paper we consider in detail the physics of grains in both ionized and neutral environments, and model these with the spectral synthesis code Cloudy. We will present a calculation of photo-electric heating and collisional cooling rates for a range of physical conditions and grain materials and for a range of grain sizes (including a realistic size distribution). A comparison of our results with benchmark calculations using the WD code will also be presented.

2. The Photo-Ionization Code Cloudy

Cloudy is a well known and widely used photo-ionization code which is publicly available at `http://www.pa.uky.edu/~gary/cloudy`. This code is not only useful for modeling fully ionized regions, but calculations can also be continued into the PDR. In order to make such a calculation realistic, the presence of a detailed grain model is required. The first grain model was introduced to Cloudy in 1990 to facilitate more accurate modeling of the Orion nebula (for a detailed description see BFM). In subsequent years, this model has undergone some revisions and extensions, but remained largely the same.

Recently, Cloudy has undergone several major upgrades, described in Ferland (2000a), Ferland (2000b), and van Hoof, Martin, & Ferland (2000). Some of these recent upgrades were aimed at improving the accuracy and versatility of Cloudy as a PDR code. These comprise an upgrade in the collision strengths of the [C I] and [O I] infrared fine-structure lines, the inclusion of a full CO model, and a comprehensive upgrade of the grain model. The latter was necessary for two reasons. First, the discovery of crystalline silicates in stellar outflows (e.g., Waters et al. 1996), and other detailed observations of grain emission features by the Infrared Space Observatory (ISO), meant that the code had to become much more flexible to allow such materials to be included in the modeling. Second, even before the ISO mission it had already become clear that the photo-electric heating and collisional cooling of the gas surrounding the grains is dominated by very small grains (possibly consisting of polycyclic aromatic hydrocarbons or PAH's). The charging of very small grains could not be modeled very accurately with the original grain model (grain physics becomes increasingly non-linear as a function of charge for smaller grains and the average potential approach of the original grain model eventually breaks down for molecule-sized grains). In view of these facts we have undertaken a comprehensive upgrade of the grain model in Cloudy. The two main aims were to make the code more flexible and versatile, and to make the modeling results more realistic. The new grain model is included in version 96 of Cloudy.[1]

[1] A beta release is currently available at `http://nimbus.pa.uky.edu/cloudy/cloudy_96.htm`

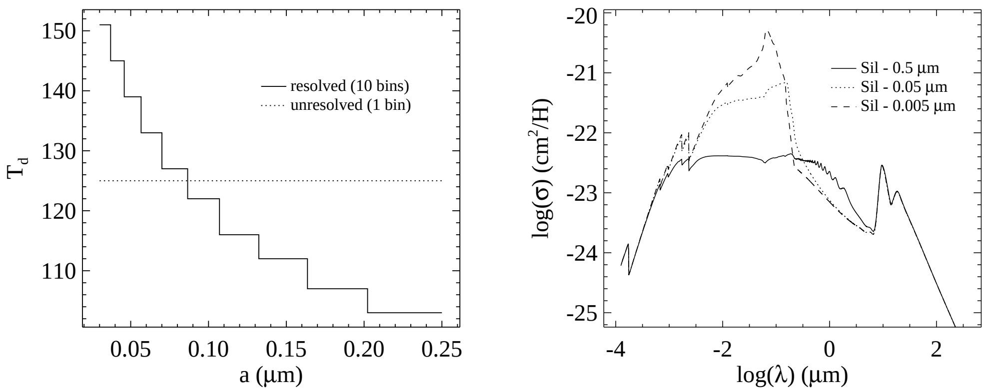

Figure 1. **Left Panel:** The average grain temperature in each size bin plotted as a function of grain size for astronomical silicate in the innermost zone of our Orion model (BFM). The solid line shows the results for a resolved size distribution, and the dotted line the results for an unresolved distribution. **Right Panel:** The absorption cross section for astronomical silicate (Draine & Lee 1984, Martin & Rouleau 1991) for three single sized grains. The dust-to-gas ratio is the same for all three species and the cross sections are normalized per hydrogen nucleus in the plasma.

3. Resolving the Grain Size Distribution

In the original grain model, opacities for a handful of grain species were hard-wired in the code. Furthermore, only a single size bin would be used for the entire size distribution. This is not a very good approximation since most grain properties depend strongly on size, e.g., the grain opacities (see the right panel of Figure 1). This approach was nevertheless adhered to in BFM because of computational restrictions.

Resolving the size distribution into many small bins improves the modeling in several ways. First, an equilibrium temperature can be calculated for each bin separately (see the left panel of Figure 1). This is important since grain emissions are a strongly non-linear function of temperature.

More importantly, resolving the size distribution also enables other improvements of the grain treatment: stochastic heating can be treated correctly for the smallest grains in the size distribution (see § 4.), and the calculations yield much more accurate results for the total photo-electric heating and collisional cooling rates of the gas by the grains (see § 5.).

To improve the model, we have implemented the following changes:

1 – We have included a Mie code for spherical particles in Cloudy. Assuming that the grains are homogeneous spheres with a given complex refractive index (optical constant) one can use Mie theory (Mie 1908) to calculate the absorption and scattering opacity. This has to be done separately for every wavelength since the refractive index depends on wavelength. Good overviews of Mie theory can be found in van de Hulst (1957), and Bohren & Huffman (1983). Our Mie code is based on the program outlined in Hansen & Travis (1974) and references therein.

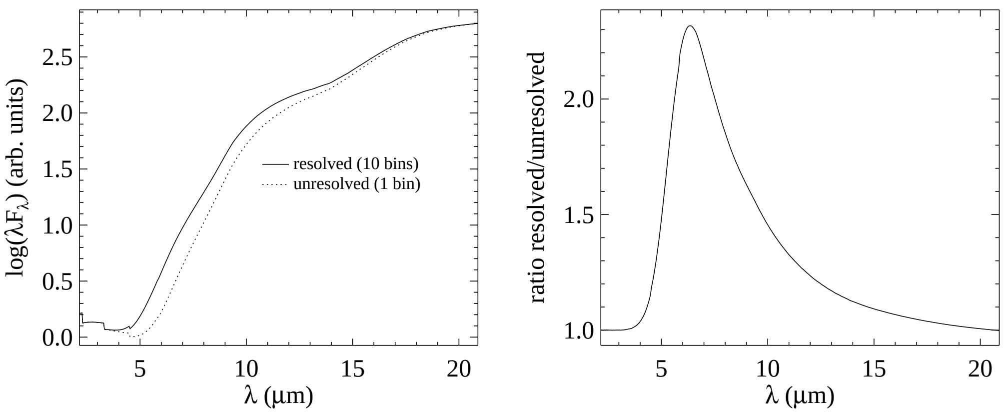

Figure 2. **Left Panel:** Model predictions for the grain emission from the face of the Orion molecular cloud complex illuminated by θ^1 Ori C, using resolved (solid line) and unresolved (dotted line) grain size distributions. Stochastic heating was turned off in these models to highlight the effect of resolving the size distribution. The flux in the center of the 10-μm feature has gone up by 45%, in the blue wing by more than a factor of two! **Right Panel:** The flux-ratio of the resolved and unresolved calculations.

The optical constants needed to run the code are read from a separate file. This allows greater freedom in the choice of grain species. Files with optical constants for a range of materials are included in the Cloudy distribution. However, the user can also supply optical constants for a completely different grain type.

2 – It is possible to use arbitrary grain size distributions. The user can either choose one of a range of preset functions (with numerous free parameters), or supply the size distribution in the form of a table. Single-sized grains can also be treated.

3 – The size distribution can be resolved in an arbitrary number of size bins (set by the user), and the absorption and scattering opacities and all the physical parameters (charge, temperature, etc.) are calculated for each bin separately.

3.1. The Dust Emission Spectrum in Orion

In Figure 2 we display the dust emission from the face of the Orion blister illuminated by θ^1 Ori C, using the BFM model with resolved and unresolved grain size distributions. These calculations include grains in the ionized region, the PDR, and fully molecular regions. Stochastic heating effects were turned off for these calculations to highlight the effect of resolving the size distribution. These effects would have been small anyway since this model is based on the BFM Orion size distribution which does not contain grains smaller than 30 nm. One can see that resolving the size distribution has a noticeable effect on the emitted spectrum since the grain emissivity depends strongly on size.

4. Stochastic Heating of Small Grains

It is well known that in conditions where the cooling time of the grain is shorter than or comparable to the average time between two significant heating events, a stochastic treatment of the grain temperature is necessary. This effect is important for grains smaller than roughly 20 nm (most notably for PAH's), and/or in regions where the photon density is very low (e.g., the diffuse ISM). The importance of this effect was first suggested by Greenberg (1968), and the topic has evolved considerably since (e.g., Desert el al. 1986, Dwek 1986), mainly focusing on efficient numerical techniques for calculating the temperature distribution of the grains. A brief history can be found in Guhathakurta & Draine (1989, hereafter GD).

Code implementing stochastic treatment of PAH's was already included in a revision to the old grain model. However, that code only worked with the two PAH species that were hardwired in Cloudy, and therefore was only infrequently used. In order to obtain accurate modeling results, the code should work on very small grains in any size distribution (which is only possible now that the size distribution has been resolved), and should include the effects automatically when they have a noticeable effect on the emitted spectrum[2]. To achieve these goals, the stochastic heating code has been extensively rewritten for the new grain model. It now works efficiently with all grain types and sizes, and under all conditions.

The original code in Cloudy was based on the algorithm of GD. The aim of this algorithm is to calculate the probability distribution of grain temperatures (or equivalently: grain enthalpies). When the code was upgraded for the current release of Cloudy, certain improvements were added to this algorithm for better performance.

The first difference with the work of GD is that we assumed $\lambda_{\rm cutoff} = \infty$ and dropped the term containing the integrated incident flux for wavelengths longer than $\lambda_{\rm cutoff}$ from the energy balance. The quantity $\lambda_{\rm cutoff}$ has no physical meaning, and was merely a numerical invention introduced by GD to avoid dealing with zero temperature grains. Our algorithm incorporates a different and more natural solution for that problem. This improved convergence of the probability distribution dramatically and helped us to avoid calculating grain enthalpy bins with extremely low probabilities. The algorithm of GD was rewritten in such a way that it is no longer necessary to set up the grain enthalpy grid *a priori*, but use an adaptive stepsize algorithm instead. This makes the algorithm much more flexible and efficient, while still guaranteeing proper convergence. The code can automatically detect when stochastic heating might be important, or when it is safe to simply use the equilibrium temperature for calculating the emitted spectrum. To highlight the importance of stochastic heating, we show in Figure 3 the spectrum emitted by a 5 nm silicate grain in typical diffuse ISM conditions with stochastic heating effects either included or not.

---

[2] In Cloudy version 96beta2 stochastic heating effects still need to be turned on explicitly by the user. Once the numerical stability of the new algorithm has been sufficiently validated, the situation will be reversed and stochastic heating effects will be included automatically unless explicitly turned off by the user.

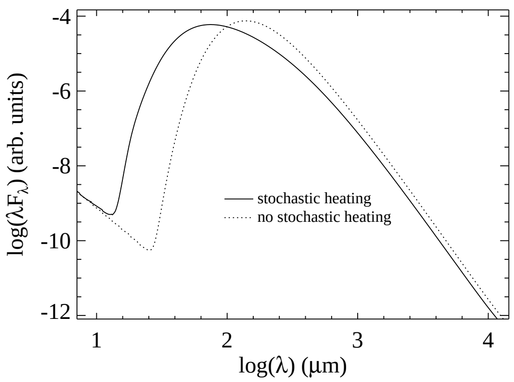

Figure 3. Model predictions for the emission from a 5 nm silicate grain in typical diffuse ISM conditions. The dotted line shows the model assuming that all grains have the same average temperature (i.e., stochastic heating effects are turned off). The solid line shows the model including stochastic effects. The model is for a hydrogen column density of 10^{20} cm^{-2}; the continuum at 10 μm is the interstellar radiation field from nearby stars.

5. Changes to the Grain Physics

We have modified certain aspects of the grain physics following the discussion in WD. Below we highlight certain aspects of these changes. A detailed description will be presented in a forthcoming paper (van Hoof et al., in preparation).

1 – We include the bandgap between the valence and conduction bands in our potential well model for silicates. This change only affects the results for negatively charged grains ($Z_{\rm g} \le -1$).

2 – Reduction of the potential barrier for negatively charged grains is included using an analytic fit to numerical calculations. Two effects are important here: quantum tunneling and the Schottky effect. Quantum theory predicts that an electron with insufficient energy to overcome a barrier still has a finite chance of tunneling through. This effect has been modeled using the WKB approximation which gives a simple analytic expression for the tunneling probability for a barrier of given width and height. Quantum tunneling is only important for small grains. For large grains the Schottky effect will dominate, which describes the lowering of the potential barrier by an image potential in the grain. This effect has been accurately modeled by Draine & Sutin (1987).

We will approximate both effects by assuming that the barrier is effectively reduced in height from $-(Z_{\rm g}+1)e^2/(4\pi\epsilon_0 a)$ to $-E_{\rm min}$. The magnitude of the combined tunneling/Schottky effect was calculated by WD. However, the fitting function they used has the wrong limiting behavior for large grains where it should asymptotically approach the classical Schottky expression. We therefore repeated these calculations using the same assumptions, but adopted a different fitting function that does exhibit the correct limiting behavior:

$$E_{\rm min} = -\,\theta_\nu \frac{e^2}{4\pi\epsilon_0 a}\left[1 - \frac{0.3}{(a/{\rm nm})^{0.45}\,\nu^{0.26}}\right], \qquad (1)$$

where $\theta_\nu[\nu = -(Z_{\rm g}+1)]$ describes the Schottky effect and is defined in Draine & Sutin (1987). The term in square brackets describes the quantum-mechanical correction. This change only affects the results for grains with $Z_{\rm g} < -1$.

3 – The treatment of the photo-electric effect has been improved, following the discussion in WD. This includes new expressions for the photo-electric yield and the energy distribution of ejected electrons.

4 – The treatment of electron sticking probabilities has been updated, again following WD. Especially for very small grains the sticking efficiency has been substantially lowered to obtain better agreement with laboratory studies of molecules. This has an important impact on the photo-electric heating rate of the gas since the electron recombination rate has to be matched by electron loss processes to preserve the charge balance. The loss processes are usually dominated by the photo-electric effect.

5 – Certain physical constants have been updated. Most notably the work function for graphite has been lowered. This results in an increased photo-electric heating rate of the gas since less of a potential barrier needs to be overcome to ionize graphite grains.

6 – The treatment of collisional heating or cooling of the grains and the gas has been improved.

Our treatment deviates from the WD code in two ways. Most importantly, we use a different grain charge model, which will be discussed in more detail in § 5.1. Secondly, we use slightly different physics for collisions between ions and grains. This only gives rise to very small differences at the 1 – 2% level when compared to the WD treatment.

5.1. The New Hybrid Grain Charge Model

The original grain model in Cloudy (which we will call the average grain potential model) is described in BFM. In that model an average grain potential is calculated by finding the potential for which the charge gain rate exactly matches the loss rate. This method was first proposed by Spitzer (1948), and is an excellent approximation for large grains. However, it is now clear that photo-electric heating and collisional cooling of the gas are dominated by very small grains. For such grains the average grain potential approximation does not work very well because grain physics becomes increasingly non-linear as a function of charge for smaller grain sizes. This fact, combined with the fact that grain charges are quantized, has led to a new approach where the charge distribution is fully resolved, and heating and cooling rates are calculated for each charge state separately (see e.g., WD). This ensures accurate results, but leads to an appreciable increase in computational overhead. This is especially the case for large grains since the width of the charge distribution increases with grain size. Hence the paradoxical situation arises that most of the computing time is spent on grains which contribute least to heating and cooling, and which are also the grains for which the average grain potential model works best!

In this paper we present a hybrid grain potential model which saves most of the computational speed of the original average grain potential model, but nevertheless gives sufficient accuracy when compared to fully resolved charge distribution calculations. The basic philosophy is that for very small grains ($a < 1$ nm) only a few charge states have a significant population. Hence we adopt the n-charge state approximation, in which all grains are treated by using exactly n contiguous charge states, independent of size. The higher n is, the more accurate the results will be (exactly how accurate will be discussed in § 5.2.). The default for Cloudy calculations is $n = 2$, but the user can request a larger number if higher precision is desired.

Since the n-charge state model does not fully resolve the charge distribution, a different algorithm from WD is needed to calculate the fractional populations f_i of each of the n charge states $Z_i \equiv Z_1 + i - 1$. These populations must first of all obey the following normalization:

$$\sum_{i=1}^{n} f_i = 1. \tag{2}$$

Secondly, we require that the electron gain rates J_i^- and electron loss rates J_i^+ summed over all charge levels match exactly:

$$\sum_{i=1}^{n} f_i (J_i^+ - J_i^-) = 0, \tag{3}$$

similar to the average grain potential model. Eqs. 2 and 3 are sufficient to determine the charge state populations if $n = 2$, but for $n > 2$ we need additional equations. These equations need to satisfy the following constraints. First, the resulting level populations should always be greater or equal zero. Second, the level populations should change continuously when the electron gain and loss rates change continuously. Third, the level populations should asymptotically approach the results from fully resolved calculations for increasing values of n. We have adopted the following algorithm:

1 – The n charge states are split up in two groups of $n - 1$ contiguous charge states. The first group contains charge states $[Z_1, Z_{n-1}]$, and the second $[Z_2, Z_n]$. The value for Z_1 is determined iteratively (see step 4).

2 – The relative level populations in the first group f_i^1 are determined using an algorithm very similar to the one used in fully resolved calculations, i.e., assume $f_1^1 = 1$, calculate $f_2^1 = f_1^1 J_1^+ / J_2^-$, $f_3^1 = f_2^1 J_2^+ / J_3^-$, etc.[3], and then re-normalize to $\sum_{i=1}^{n-1} f_i^1 = 1$. We use an analogous procedure for the populations f_i^2 of the second group for $i \in [2, n]$.

3 – Determine for both groups the net charging rate

$$J_k = \sum_{i=k}^{n-2+k} f_i^k (J_i^+ - J_i^-) \quad (k = 1, 2). \tag{4}$$

4 – Iterate Z_1 and repeat steps 1 – 3 until $J_1 \times J_2 \leq 0$. Then find $0 \leq \alpha \leq 1$ such that

$$\alpha J_1 + (1 - \alpha) J_2 = 0. \tag{5}$$

[3]Note that this procedure is not correct for charge transfer with multiply charged ions. In order to avoid having to solve a full set of linear equations, we will approximate this process as multiple single-charge-transfer events. The resulting errors are expected to be small as collision rates for multiply charged ions are usually quite low because their velocities are small compared to electrons. The collision rates are normally suppressed even further by the positive grain charge.

5 – Determine the final charge state populations as follows

$$f_i = \alpha\, f_i^1 + (1-\alpha)\, f_i^2 \quad (\text{with } f_n^1 \equiv 0, f_1^2 \equiv 0). \tag{6}$$

One can verify that this algorithm satisfies all constraints.

The hybrid grain potential model is efficient because it avoids the overhead for large grains, while still giving accurate results for both small and large grains. An added bonus is that most of the time an excellent initial estimate for Z_1 can be derived from the previous zone, reducing the overhead even further. The model works for very small grains because only few charge states are populated and it can reconstruct the actual charge distribution. It works for large grains because the grain potential distribution approaches a delta function for increasing grain size (as opposed to the charge distribution which becomes ever wider). Our method therefore asymptotically approaches the average grain potential model, which we already know is very accurate for large grains.

5.2. Validating the Hybrid Grain Charge Model

In order to validate the new grain charge model, we calculated the photo-electric heating and collisional cooling rates for a range of physical conditions, two grain species, and a wide range of grain sizes (including a realistic size distribution). We then compared these calculations with benchmark results from the WD code, which fully resolves the charge distribution.

We model the physical conditions with simple assumptions: the plasma only contains hydrogen, the electron temperature and density are fixed at prescribed values, the incident spectrum is assumed to be a blackbody (either full in the warm ISM and ionized cases, or cut off at 13.6 eV in the cold ISM and PDR cases). To allow for an accurate comparison, both codes used the same optical constants for classical graphite and astronomical silicate (Draine & Lee 1984). In Cloudy the photo-electric heating by local diffuse emission was switched off, as well as thermionic emissions and collisional cooling by neutral hydrogen since these are not treated in the WD code. The WD code was modified according to Eq. 1. Except for the grain charge model, the treatment of the grain physics in Cloudy and the WD code are very similar.

We present results for selected single sized grains, as well as a realistic reconstruction of the ISM grain size distribution (labeled A6) taken from Weingartner & Draine (2001b). In the ISM and H II region cases we used a standard mix of graphite and silicate as prescribed by Weingartner & Draine (2001b)[4]. In the planetary nebula cases, we made separate models for either graphite or silicate as these two species are not expected to coexist spatially in the nebular material on theoretical grounds[5].

---

[4]Note that the A6 size distribution was derived by matching the extinction curve using grain opacities defined in Li & Draine (2001). In this study we use the same size distribution, but use opacities from Draine & Lee (1984) instead, which is not consistent. This inconsistency is irrelevant for our purposes.

[5]Note that spectroscopy of planetary nebulae by ISO has revealed a surprisingly large number of cases that show both silicate and graphitic dust features. One famous example is NGC 6302 (Molster et al. 2001). It is however usually assumed that the two species reside in different parts of the nebula.

Table 1. Physical parameters for the benchmark models. Symbols have their usual meaning, G is the intensity of the radiation field and $G_0 = 1.6\times10^{-6}$ W m^{-2}, integrated between 6 and 13.6 eV, is the Habing intensity. T_c is the color temperature of the radiation field.

	ISM		H II		PN	
	warm	cold	ionized	PDR	ionized	PDR
T_c/kK	35	35	50	50	250	250
$\log(G/G_0)$	0	0	5	5	5	5
$\log(n_H/\mathrm{cm}^{-3})$	0	1	4	4	4	4
$\log(n_e/\mathrm{cm}^{-3})$	0	−2	4	1	4	1
T_e/kK	9	0.1	9	1	20	1

The physical parameters for the models are listed in Table 1; the results of the calculation are presented in Tables 2, 3, and 4.

5.3. Discussion

A summary of the comparison of the photo-electric heating and collisional cooling rates from Tables 2, 3, and 4 is given in Table 5. In general the results are in excellent agreement, with only a few outliers for single sized grains in the $n = 2$ and $n = 3$ cases. The results for the size distribution cases always agree to better than 25%, even for $n = 2$. This is well within the accuracy with which we know grain physics to date. There are still major uncertainties in the photo-electric yields and the sticking efficiency for electrons, both of which have a strong effect on the photo-electric heating rate. Also the work function and bandgap for astrophysical grain materials are poorly known and can have a strong effect as well. This is unfortunate since photo-electric heating and collisional cooling in photoionized environments are important effects. All these uncertainties mainly stem from the fact that the composition of interstellar grains is still poorly known.

From Table 5 one can see that the collisional cooling rates usually are in better agreement than the photo-electric heating rates for a given set of physical parameters. It is furthermore clear that the accuracy of the n-charge state approximation increases as n increases, as should be expected. Closer inspection of Tables 2, 3, and 4 for single sized grains reveals that the largest errors in the $n = 2$ and $n = 3$ cases are for the 0.5 nm grains, for $n = 4$ for either 2 nm or 10 nm grains, and for $n = 5$ for 10 nm grains, i.e., the grain size for which the errors are largest shifts upwards for higher values of n. This is expected since the n-charge state approximation will fully resolve the charge distribution of the smallest grains for $n > 3$. Note that the results for the 100 nm grains are always in excellent agreement, even when $n = 2$, despite the fact that the actual charge distribution is much wider than that.

The agreement between the Cloudy and the WD results is very satisfactory for realistic size distributions, and should be sufficient for all realistic astrophysical applications. Therefore the hybrid grain charge model presented above (with $n = 2$) will be the default for Cloudy modeling.

Table 2: Comparison of the heating and cooling rates (in $\mathrm{W\,m^{-3}}$) for the ISM cases between the fully resolved charge-state calculations by Weingartner & Draine (2001a, WD) and the n-charge state calculations with Cloudy 96beta2 (indicated as CLDn). The difference Δ = CLDn/WD − 1 (in percent) is also indicated. 1.576(−25) stands for 1.576×10^{-25}. The calculations are for a range of single sized grains (indicated in nm in the first column of each WD entry), and for an A6 size distribution, which stands for the $R_V = 3.1$, case A, $b_{\mathrm{C}} = 6.0\times10^{-5}$ size distribution defined in Weingartner & Draine (2001b). The A6 size distribution contains both graphite and silicate grains.

	Heating								Cooling							
	warm				cold				warm				cold			
	graphite	Δ	silicate	Δ	graphite	Δ	silicate	Δ	graphite	Δ	silicate	Δ	graphite	Δ	silicate	Δ
WD 0.5	1.576(−25)		6.004(−26)		1.395(−26)		4.044(−27)		1.582(−25)		1.435(−25)		5.109(−29)		2.912(−29)	
CLD2	1.556(−25)	−1.3	5.914(−26)	−1.5	1.108(−26)	−20.6	1.798(−27)	−55.5	1.599(−25)	+1.1	1.445(−25)	+0.7	4.851(−29)	−5.1	2.239(−29)	−23.1
CLD3	1.561(−25)	−1.0	5.928(−26)	−1.3	1.167(−26)	−16.3	2.836(−27)	−29.9	1.594(−25)	+0.8	1.443(−25)	+0.6	4.900(−29)	−4.1	2.549(−29)	−12.5
CLD4	1.576(−25)	−0.0	5.998(−26)	−0.1	1.357(−26)	−2.7	4.018(−27)	−0.6	1.578(−25)	−0.2	1.431(−25)	−0.3	5.064(−29)	−0.9	2.900(−29)	−0.4
CLD5	1.577(−25)	+0.0	5.999(−26)	−0.1	1.391(−26)	−0.3	4.019(−27)	−0.6	1.578(−25)	−0.2	1.431(−25)	−0.3	5.094(−29)	−0.3	2.900(−29)	−0.4
WD 1.0	1.740(−25)		6.431(−26)		1.437(−26)		4.652(−27)		9.606(−26)		8.705(−26)		4.725(−29)		3.388(−29)	
CLD2	1.637(−25)	−5.9	6.119(−26)	−4.9	1.354(−26)	−5.8	3.981(−27)	−14.4	9.935(−26)	+3.4	8.982(−26)	+3.2	4.686(−29)	−0.8	3.201(−29)	−5.5
CLD3	1.678(−25)	−3.6	6.293(−26)	−2.1	1.354(−26)	−5.8	4.064(−27)	−12.6	9.810(−26)	+2.1	8.833(−26)	+1.5	4.688(−29)	−0.8	3.223(−29)	−4.9
CLD4	1.706(−25)	−2.0	6.386(−26)	−0.7	1.382(−26)	−3.9	4.455(−27)	−4.2	9.711(−26)	+1.1	8.752(−26)	+0.5	4.691(−29)	−0.7	3.327(−29)	−1.8
CLD5	1.723(−25)	−1.0	6.425(−26)	−0.1	1.420(−26)	−1.2	4.620(−27)	−0.7	9.640(−26)	+0.4	8.704(−26)	−0.0	4.698(−29)	−0.6	3.373(−29)	−0.4
WD 2.0	1.541(−25)		5.684(−26)		1.201(−26)		4.415(−27)		6.112(−26)		5.089(−26)		3.645(−29)		3.072(−29)	
CLD2	1.489(−25)	−3.4	5.413(−26)	−4.8	1.188(−26)	−1.1	4.231(−27)	−4.2	6.391(−26)	+4.6	5.349(−26)	+5.1	3.653(−29)	+0.2	3.027(−29)	−1.5
CLD3	1.496(−25)	−3.0	5.478(−26)	−3.6	1.185(−26)	−1.4	4.246(−27)	−3.8	6.345(−26)	+3.8	5.292(−26)	+4.0	3.645(−29)	+0.0	3.031(−29)	−1.4
CLD4	1.508(−25)	−2.2	5.536(−26)	−2.6	1.183(−26)	−1.5	4.269(−27)	−3.3	6.273(−26)	+2.6	5.231(−26)	+2.8	3.638(−29)	−0.2	3.036(−29)	−1.2
CLD5	1.520(−25)	−1.4	5.593(−26)	−1.6	1.184(−26)	−1.5	4.328(−27)	−2.0	6.205(−26)	+1.5	5.169(−26)	+1.6	3.631(−29)	−0.4	3.048(−29)	−0.8
WD 10	4.822(−26)		1.818(−26)		4.735(−27)		1.556(−27)		1.537(−26)		1.261(−26)		1.635(−29)		1.208(−29)	
CLD2	4.772(−26)	−1.1	1.789(−26)	−1.6	4.667(−27)	−1.4	1.514(−27)	−2.7	1.674(−26)	+8.9	1.277(−26)	+1.3	1.634(−29)	−0.1	1.198(−29)	−0.8
CLD3	4.773(−26)	−1.0	1.792(−26)	−1.4	4.668(−27)	−1.4	1.517(−27)	−2.5	1.663(−26)	+8.2	1.276(−26)	+1.2	1.633(−29)	−0.1	1.198(−29)	−0.8
CLD4	4.779(−26)	−0.9	1.793(−26)	−1.4	4.671(−27)	−1.4	1.519(−27)	−2.4	1.616(−26)	+5.2	1.276(−26)	+1.2	1.633(−29)	−0.1	1.198(−29)	−0.8
CLD5	4.784(−26)	−0.8	1.796(−26)	−1.2	4.673(−27)	−1.3	1.523(−27)	−2.2	1.591(−26)	+3.5	1.276(−26)	+1.2	1.633(−29)	−0.1	1.199(−29)	−0.7
WD 100	1.832(−27)		7.965(−28)		2.825(−28)		9.453(−29)		8.853(−28)		7.931(−28)		9.547(−31)		7.524(−31)	
CLD2	1.830(−27)	−0.1	7.947(−28)	−0.2	2.808(−28)	−0.6	9.389(−29)	−0.7	8.849(−28)	−0.0	7.930(−28)	−0.0	9.471(−31)	−0.8	7.472(−31)	−0.7
CLD3	1.829(−27)	−0.1	7.947(−28)	−0.2	2.807(−28)	−0.6	9.389(−29)	−0.7	8.853(−28)	+0.0	7.930(−28)	−0.0	9.476(−31)	−0.7	7.472(−31)	−0.7
CLD4	1.829(−27)	−0.1	7.947(−28)	−0.2	2.807(−28)	−0.6	9.389(−29)	−0.7	8.853(−28)	+0.0	7.930(−28)	−0.0	9.476(−31)	−0.7	7.472(−31)	−0.7
CLD5	1.829(−27)	−0.1	7.947(−28)	−0.2	2.807(−28)	−0.6	9.390(−29)	−0.7	8.853(−28)	+0.0	7.930(−28)	−0.0	9.476(−31)	−0.7	7.472(−31)	−0.7
WD A6	5.120(−26)				4.437(−27)				3.900(−26)				1.826(−29)			
CLD2	4.930(−26)	−3.7			3.897(−27)	−12.2			3.920(−26)	+0.5			1.761(−29)	−3.5		
CLD3	4.964(−26)	−3.1			3.990(−27)	−10.1			3.905(−26)	+0.1			1.771(−29)	−3.0		
CLD4	5.029(−26)	−1.8			4.289(−27)	−3.3			3.873(−26)	−0.7			1.799(−29)	−1.5		
CLD5	5.065(−26)	−1.1			4.366(−27)	−1.6			3.858(−26)	−1.1			1.804(−29)	−1.2		

Table 3: Same as Table 2, except these are the results for the H II region cases.

	Heating								Cooling							
	ionized				PDR				ionized				PDR			
	graphite	Δ	silicate	Δ	graphite	Δ	silicate	Δ	graphite	Δ	silicate	Δ	graphite	Δ	silicate	Δ
WD 0.5	1.786(−25)		9.205(−26)		2.354(−28)		1.140(−28)		3.911(−26)		2.827(−26)		1.963(−29)		1.153(−29)	
CLD2	1.621(−25)	−9.2	7.983(−26)	−13.3	1.896(−28)	−19.5	1.044(−28)	−8.5	3.903(−26)	−0.2	2.887(−26)	+2.1	1.826(−29)	−6.9	1.086(−29)	−5.8
CLD3	1.634(−25)	−8.5	8.593(−26)	−6.6	1.997(−28)	−15.1	1.056(−28)	−7.4	3.915(−26)	+0.1	2.841(−26)	+0.5	1.864(−29)	−5.0	1.095(−29)	−5.0
CLD4	1.693(−25)	−5.2	8.991(−26)	−2.3	2.218(−28)	−5.8	1.126(−28)	−1.3	3.913(−26)	+0.1	2.814(−26)	−0.5	1.940(−29)	−1.1	1.145(−29)	−0.7
CLD5	1.751(−25)	−2.0	9.173(−26)	−0.3	2.350(−28)	−0.2	1.138(−28)	−0.2	3.898(−26)	−0.3	2.815(−26)	−0.4	1.956(−29)	−0.3	1.147(−29)	−0.5
WD 1.0	1.608(−25)		8.741(−26)		1.292(−28)		6.079(−29)		3.307(−26)		2.237(−26)		1.532(−29)		9.703(−30)	
CLD2	1.498(−25)	−6.8	8.326(−26)	−4.8	1.044(−28)	−19.2	4.923(−29)	−19.0	3.303(−26)	−0.1	2.229(−26)	−0.4	1.495(−29)	−2.4	9.512(−30)	−2.0
CLD3	1.520(−25)	−5.5	8.358(−26)	−4.4	1.080(−28)	−16.4	5.202(−29)	−14.4	3.303(−26)	−0.1	2.236(−26)	−0.1	1.497(−29)	−2.2	9.548(−30)	−1.6
CLD4	1.532(−25)	−4.7	8.450(−26)	−3.3	1.193(−28)	−7.7	5.953(−29)	−2.1	3.303(−26)	−0.1	2.237(−26)	+0.0	1.509(−29)	−1.4	9.646(−30)	−0.6
CLD5	1.554(−25)	−3.4	8.569(−26)	−2.0	1.258(−28)	−2.6	5.999(−29)	−1.3	3.304(−26)	−0.1	2.234(−26)	−0.2	1.523(−29)	−0.5	9.662(−30)	−0.4
WD 2.0	1.176(−25)		6.960(−26)		6.401(−29)		2.926(−29)		2.515(−26)		1.614(−26)		1.004(−29)		6.336(−30)	
CLD2	1.123(−25)	−4.5	6.793(−26)	−2.4	4.952(−29)	−22.6	2.418(−29)	−17.4	2.512(−26)	−0.1	1.600(−26)	−0.9	9.804(−30)	−2.4	6.158(−30)	−2.8
CLD3	1.127(−25)	−4.2	6.796(−26)	−2.4	5.395(−29)	−15.7	2.433(−29)	−16.9	2.511(−26)	−0.1	1.600(−26)	−0.9	9.878(−30)	−1.6	6.159(−30)	−2.8
CLD4	1.130(−25)	−3.9	6.825(−26)	−1.9	5.788(−29)	−9.6	2.667(−29)	−8.9	2.511(−26)	−0.1	1.603(−26)	−0.7	9.935(−30)	−1.0	6.236(−30)	−1.6
CLD5	1.137(−25)	−3.3	6.845(−26)	−1.6	6.150(−29)	−3.9	2.845(−29)	−2.8	2.511(−26)	−0.1	1.605(−26)	−0.6	9.975(−30)	−0.6	6.298(−30)	−0.6
WD 10	2.910(−26)		1.663(−26)		8.186(−30)		3.710(−30)		6.361(−27)		4.017(−27)		2.180(−30)		1.348(−30)	
CLD2	2.916(−26)	+0.2	1.672(−26)	+0.5	7.469(−30)	−8.8	3.308(−30)	−10.8	6.306(−27)	−0.9	3.965(−27)	−1.3	2.164(−30)	−0.7	1.332(−30)	−1.2
CLD3	2.916(−26)	+0.2	1.672(−26)	+0.6	7.588(−30)	−7.3	3.380(−30)	−8.9	6.306(−27)	−0.9	3.965(−27)	−1.3	2.165(−30)	−0.7	1.334(−30)	−1.0
CLD4	2.917(−26)	+0.2	1.673(−26)	+0.6	7.649(−30)	−6.6	3.422(−30)	−7.8	6.306(−27)	−0.9	3.965(−27)	−1.3	2.166(−30)	−0.6	1.335(−30)	−1.0
CLD5	2.918(−26)	+0.3	1.673(−26)	+0.6	7.759(−30)	−5.2	3.499(−30)	−5.7	6.306(−27)	−0.9	3.966(−27)	−1.3	2.168(−30)	−0.6	1.337(−30)	−0.8
WD 100	2.199(−27)		9.966(−28)		9.131(−31)		3.724(−31)		3.850(−28)		2.475(−28)		1.903(−31)		1.154(−31)	
CLD2	2.202(−27)	+0.1	9.973(−28)	+0.1	9.132(−31)	+0.0	3.716(−31)	−0.2	3.843(−28)	−0.2	2.466(−28)	−0.3	1.895(−31)	−0.4	1.147(−31)	−0.6
CLD3	2.202(−27)	+0.1	9.973(−28)	+0.1	9.133(−31)	+0.0	3.725(−31)	+0.0	3.843(−28)	−0.2	2.466(−28)	−0.3	1.895(−31)	−0.4	1.147(−31)	−0.6
CLD4	2.202(−27)	+0.1	9.974(−28)	+0.1	9.133(−31)	+0.0	3.726(−31)	+0.0	3.843(−28)	−0.2	2.466(−28)	−0.3	1.895(−31)	−0.4	1.147(−31)	−0.6
CLD5	2.202(−27)	+0.1	9.974(−28)	+0.1	9.134(−31)	+0.0	3.726(−31)	+0.0	3.843(−28)	−0.2	2.466(−28)	−0.3	1.895(−31)	−0.4	1.147(−31)	−0.6
WD A6	5.073(−26)				4.643(−29)				1.116(−26)				5.150(−30)			
CLD2	4.691(−26)	−7.5			3.569(−29)	−23.1			1.103(−26)	−1.1			4.960(−30)	−3.7		
CLD3	4.738(−26)	−6.6			3.884(−29)	−16.3			1.104(−26)	−1.1			5.001(−30)	−2.9		
CLD4	4.836(−26)	−4.7			4.436(−29)	−4.5			1.104(−26)	−1.1			5.069(−30)	−1.6		
CLD5	4.932(−26)	−2.8			4.577(−29)	−1.4			1.103(−26)	−1.2			5.086(−30)	−1.2		

Table 4: Same as Table 2, except these are the results for the planetary nebula cases. Results for the silicate and graphite components of the A6 distribution are shown separately.

	Heating								Cooling							
	ionized				PDR				ionized				PDR			
	graphite	Δ	silicate	Δ	graphite	Δ	silicate	Δ	graphite	Δ	silicate	Δ	graphite	Δ	silicate	Δ
WD 0.5	1.163(−24)		2.048(−24)		2.268(−28)		1.157(−28)		1.831(−25)		2.100(−25)		2.037(−29)		1.196(−29)	
CLD2	1.145(−24)	−1.6	2.013(−24)	−1.7	1.585(−28)	−30.1	1.007(−28)	−13.0	1.764(−25)	−3.7	2.055(−25)	−2.1	1.850(−29)	−9.2	1.099(−29)	−8.2
CLD3	1.146(−24)	−1.5	2.016(−24)	−1.6	1.845(−28)	−18.6	1.038(−28)	−10.3	1.772(−25)	−3.3	2.059(−25)	−2.0	1.927(−29)	−5.4	1.119(−29)	−6.5
CLD4	1.148(−24)	−1.4	2.019(−24)	−1.4	2.163(−28)	−4.6	1.147(−28)	−0.9	1.781(−25)	−2.7	2.062(−25)	−1.8	2.020(−29)	−0.9	1.187(−29)	−0.7
CLD5	1.150(−24)	−1.2	2.024(−24)	−1.2	2.267(−28)	−0.1	1.156(−28)	−0.1	1.794(−25)	−2.0	2.069(−25)	−1.5	2.030(−29)	−0.4	1.189(−29)	−0.6
WD 1.0	1.016(−24)		1.790(−24)		1.229(−28)		6.030(−29)		1.523(−25)		1.793(−25)		1.573(−29)		9.953(−30)	
CLD2	1.010(−24)	−0.6	1.772(−24)	−1.0	1.015(−28)	−17.4	5.124(−29)	−15.0	1.492(−25)	−2.0	1.773(−25)	−1.2	1.529(−29)	−2.7	9.813(−30)	−1.4
CLD3	1.010(−24)	−0.6	1.773(−24)	−1.0	1.016(−28)	−17.3	5.269(−29)	−12.6	1.492(−25)	−2.0	1.774(−25)	−1.1	1.530(−29)	−2.7	9.826(−30)	−1.3
CLD4	1.011(−24)	−0.5	1.774(−24)	−0.9	1.120(−28)	−8.8	5.879(−29)	−2.5	1.495(−25)	−1.8	1.774(−25)	−1.1	1.550(−29)	−1.4	9.881(−30)	−0.7
CLD5	1.011(−24)	−0.5	1.775(−24)	−0.9	1.208(−28)	−1.7	5.960(−29)	−1.2	1.497(−25)	−1.7	1.776(−25)	−1.0	1.566(−29)	−0.4	9.913(−30)	−0.4
WD 2.0	7.829(−25)		1.392(−24)		5.953(−29)		2.779(−29)		1.146(−25)		1.386(−25)		1.028(−29)		6.512(−30)	
CLD2	7.930(−25)	+1.3	1.400(−24)	+0.5	4.456(−29)	−25.1	2.232(−29)	−19.7	1.123(−25)	−2.0	1.366(−25)	−1.4	1.006(−29)	−2.1	6.295(−30)	−3.3
CLD3	7.931(−25)	+1.3	1.400(−24)	+0.5	5.043(−29)	−15.3	2.319(−29)	−16.6	1.124(−25)	−2.0	1.366(−25)	−1.4	1.013(−29)	−1.5	6.343(−30)	−2.6
CLD4	7.932(−25)	+1.3	1.400(−24)	+0.6	5.436(−29)	−8.7	2.530(−29)	−9.0	1.124(−25)	−1.9	1.366(−25)	−1.4	1.017(−29)	−1.0	6.428(−30)	−1.3
CLD5	7.933(−25)	+1.3	1.400(−24)	+0.6	5.678(−29)	−4.6	2.728(−29)	−1.9	1.124(−25)	−1.9	1.367(−25)	−1.4	1.021(−29)	−0.7	6.481(−30)	−0.5
WD 10	2.993(−25)		5.317(−25)		7.394(−30)		3.390(−30)		3.701(−26)		4.601(−26)		2.217(−30)		1.375(−30)	
CLD2	3.001(−25)	+0.2	5.317(−25)	+0.0	6.664(−30)	−9.9	2.975(−30)	−12.2	3.683(−26)	−0.5	4.584(−26)	−0.4	2.201(−30)	−0.7	1.359(−30)	−1.2
CLD3	3.001(−25)	+0.3	5.318(−25)	+0.0	6.804(−30)	−8.0	3.058(−30)	−9.8	3.683(−26)	−0.5	4.584(−26)	−0.4	2.202(−30)	−0.7	1.361(−30)	−1.0
CLD4	3.001(−25)	+0.3	5.318(−25)	+0.0	6.870(−30)	−7.1	3.116(−30)	−8.1	3.683(−26)	−0.5	4.584(−26)	−0.4	2.203(−30)	−0.6	1.363(−30)	−0.9
CLD5	3.001(−25)	+0.3	5.318(−25)	+0.0	6.991(−30)	−5.5	3.189(−30)	−5.9	3.683(−26)	−0.5	4.584(−26)	−0.4	2.205(−30)	−0.6	1.365(−30)	−0.8
WD 100	5.850(−26)		5.299(−26)		8.301(−31)		3.376(−31)		5.562(−27)		3.895(−27)		1.950(−31)		1.187(−31)	
CLD2	5.865(−26)	+0.3	5.303(−26)	+0.1	8.318(−31)	+0.2	3.406(−31)	+0.9	5.551(−27)	−0.2	3.888(−27)	−0.2	1.942(−31)	−0.4	1.180(−31)	−0.6
CLD3	5.865(−26)	+0.3	5.303(−26)	+0.1	8.335(−31)	+0.4	3.415(−31)	+1.2	5.551(−27)	−0.2	3.888(−27)	−0.2	1.942(−31)	−0.4	1.179(−31)	−0.6
CLD4	5.865(−26)	+0.3	5.303(−26)	+0.1	8.336(−31)	+0.4	3.416(−31)	+1.2	5.551(−27)	−0.2	3.888(−27)	−0.2	1.942(−31)	−0.4	1.180(−31)	−0.6
CLD5	5.865(−26)	+0.3	5.303(−26)	+0.1	8.336(−31)	+0.4	3.417(−31)	+1.2	5.551(−27)	−0.2	3.888(−27)	−0.2	1.942(−31)	−0.4	1.180(−31)	−0.6
WD A6	3.100(−25)		2.717(−25)		4.159(−29)		3.454(−30)		4.476(−26)		2.333(−26)		4.430(−30)		8.660(−31)	
CLD2	3.047(−25)	−1.7	2.709(−25)	−0.3	3.298(−29)	−20.7	2.802(−30)	−18.9	4.312(−26)	−3.7	2.310(−26)	−1.0	4.272(−30)	−3.6	8.439(−31)	−2.5
CLD3	3.048(−25)	−1.7	2.710(−25)	−0.3	3.501(−29)	−15.8	3.036(−30)	−12.1	4.319(−26)	−3.5	2.311(−26)	−0.9	4.296(−30)	−3.0	8.517(−31)	−1.6
CLD4	3.051(−25)	−1.6	2.710(−25)	−0.3	4.012(−29)	−3.5	3.294(−30)	−4.6	4.338(−26)	−3.1	2.311(−26)	−0.9	4.354(−30)	−1.7	8.597(−31)	−0.7
CLD5	3.054(−25)	−1.5	2.711(−25)	−0.2	4.117(−29)	−1.0	3.384(−30)	−2.0	4.357(−26)	−2.7	2.312(−26)	−0.9	4.365(−30)	−1.5	8.619(−31)	−0.5

Table 5. Summary of the comparison between the Cloudy n-charge state calculations (indicated by CLDn) and the benchmark calculations with the WD code. All entries are differences CLDn/WD − 1 in percent.

	Heating				Cooling			
	single size		size distr.		single size		size distr.	
	median	worst	median	worst	median	worst	median	worst
CLD2	−3.03	−55.5	−9.85	−23.1	−0.77	−23.1	−3.05	−3.7
CLD3	−2.44	−29.9	−8.34	−16.3	−0.72	−12.5	−2.27	−3.5
CLD4	−1.40	−9.6	−3.43	−4.7	−0.65	+5.2	−1.30	−3.1
CLD5	−0.75	−5.9	−1.45	−2.8	−0.44	+3.5	−1.21	−2.7

6. Outlook

The rapid increase in computing power over the past decades has made it possible now to build detailed grain models that can be run in a modest amount of time. Computing power is therefore not a limiting factor anymore, and the gaps in our knowledge of grain physics are almost exclusively what is hampering progress at the moment. These gaps need to be filled in, both through laboratory work, and observations of interstellar and circumstellar grains. Some of the key areas have already been indicated above. They include a better understanding of the exact chemical composition of the grains, and the size distribution as a function of environment, as well as the corresponding physical properties (electron and ion sticking efficiencies, photo-electric yields, work functions, and bandgaps) for realistic astronomical materials. Depletion of trace elements onto grains should also be understood better since that has an important effect on the abundances of the gas in which the grains have been formed and alters the emitted spectrum and cooling rate of the gas. An improved model of the life cycle of dust (including grain formation, coagulation, and destruction in the ISM, as well as the formation of crystalline materials in circumstellar envelopes, which was one of the great surprises from the ISO mission) should go hand in hand with the above improvements. In the long run theory combined with laboratory experiment should move towards building full quantum-mechanical models of very small grains, which are now treated by heuristic, semi-classical methods. Currently the complexity of such models is still computationally prohibitive.

We are currently using Cloudy to model the Ney-Allen nebula (Ney & Allen 1969), which is situated close to θ^1 Ori D. The silicate emission from this nebula was used (combined with data from long period variable stars) as a template to define astronomical silicate (Draine & Lee 1984). Now this effort will come full circle by using the derived astronomical silicate data to model the Ney-Allen nebula. This will be an important test of our understanding of interstellar grains. The improvements presented above are important for this effort since the silicate 10 μm feature is situated in the Wien tail of the emission, and effects from resolving the size distribution (see Fig. 2) as well as temperature spiking of very small grains are important. This work will be presented in a forthcoming paper (van Hoof et al., in preparation).

Acknowledgments. We wish to acknowledge financial support by the National Science Foundation through grant no. AST–0071180, and NASA through its LTSA program, NAG 5–3223. This research was also supported in part by the Natural Sciences and Engineering Research Council of Canada. J.C.W. acknowledges support from an NSF International Research Fellowship.

References

Bakes, E. L. O., & Tielens, A. G. G. M. 1994, ApJ, 427, 822

Baldwin, J. A., Ferland, G. J., Martin, P. G., Corbin, M. R., Cota, S. A., Peterson, B. M., & Slettebak, A. 1991, ApJ, 374, 580 (BFM)

Bohren, C. F., & Huffman, D. R. 1983, Absorption and Scattering of Light by Small Particles (Ney York: Wiley)

Borkowski, K. J., & Harrington, J. P. 1991, ApJ, 379, 168

Desert, F. X., Boulanger, F., & Shore, S. N. 1986, A&A, 160, 295

Draine, B. T., & Lee, H. M. 1984, ApJ, 285, 89

Draine, B. T., & Sutin, B. 1987, ApJ, 320, 803

Dwek, E. 1986, ApJ, 302, 363

Ferland, G. J. 2000a, in Astronomical Data Analysis Software and Systems IX, eds. Manset, N., Veillet, C., & Crabtree, D., ASP Conference Series, Vol. 216, (San Francisco: Astronomical Society of the Pacific), p. 32.

Ferland, G. J. 2000b, Rev. Mex. Astr. Astrof. (Serie de Conferencias), 9, 153

Greenberg, J. M., 1968, in Stars and Stellar Systems, Vol. 7, Nebulae and Interstellar Matter, eds. Middlehurst, B. M., & Aller, L. H., (Chicago: Chicago University Press), p. 221

Guhathakurta, P., & Draine, B. T. 1989, ApJ, 345, 230 (GD)

Hansen, J. E., & Travis, L. D. 1974, Space Sci. Rev., 16, 527

Li, A., & Draine, B. T. 2001, ApJ, in press (astro-ph/0011319)

Maciel, W. J., & Pottasch, S. R. 1982, A&A, 86, 380

Martin, P. G., & Rouleau, F. 1991, in Extreme Ultraviolet Astronomy, eds. Malina, R. F., & Bowyer, S., (New York: Pergamon Press), p. 341

Mie, G. 1908, Ann. Phys., 25, 377

Molster, F. J., et al. 2001, A&A, 372, 165

Ney, E. P., & Allen, D. A. 1969, ApJ, 155, L193

Spitzer, L. 1948, ApJ, 107, 6

Tielens, A. G. G. M., & Hollenbach, D. J. 1985, ApJ, 291, 722

van de Hulst, H. C. 1957, Light Scattering by Small Particles, (Ney York: Wiley)

van Hoof, P. A. M., Martin, P. G., & Ferland, G. J. 2000, in Cosmic Evolution and Galaxy Formation: Structure, Interactions, and Feedback, eds. Franco, J., Terlevich, E., López-Cruz, O., & Aretxaga, I., ASP Conference Series, Vol. 215, (San Francisco: Astronomical Society of the Pacific), p. 220 (extended version: astro-ph/0001196)

Waters, L. B. F. M., et al. 1996, A&A, 315, L361

Weingartner, J. C., & Draine, B. T. 2001a, ApJS, 134, 263 (WD)
Weingartner, J. C., & Draine, B. T. 2001b, ApJ, 548, 296